Opto-Electronic Advances

CN 51-1781/TN ISSN 2096-4579 (Print) ISSN 2097-3993 (Online)

High-precision multi-focus laser sculpting of microstructured glass

Kang Xu, Peilin Huang, Lingyu Huang, Li Yao, Zongyao Li, Jiantao Chen, Li Zhang and Shaolin Xu

Citation: Xu K, Huang PL, Huang LY, et al. High-precision multi-focus laser sculpting of microstructured glass. *Opto-Electron Adv* **7**, 240082(2024).

https://doi.org/10.29026/oea.2025.240082

Received: 14 April 2024; Accepted: 22 July 2024; Published online: 9 October 2024

Opto-Electronic Advances

Article

November 2024, Vol. 7, No. 11

DOI: 10.29026/oea.2025.240082 CSTR: 32247.14.oea.2025.240082

High-precision multi-focus laser sculpting of microstructured glass

Kang Xu[1†], Peilin Huang[1†], Lingyu Huang[1], Li Yao[1], Zongyao Li[1], Jiantao Chen[1], Li Zhang[2] and Shaolin Xu[1*]

Precision sculpting of glass with defined surface microstructures is vital due to the miniaturization and integration of glass-based devices, while it is still challenging as the high brittleness of glass. We here create a three-dimensional multi-focus laser for glass micro-sculpting through a beam-shaping technology based on the superposition of lens and grating phase diagrams. The multi-focus laser modification in tandem with chemical etching enables the fabrication of glass microstructures with highly adjustable profiles. Refractive-index-induced deviations are migrated via algorithm correction to ensure multi-focus positional accuracy. Energy un-uniformity due to equidistant laser spots arrangement is eliminated through their coordinate randomization following the target profiles. Finally, uniform laser spots with a proper point-to-point distance create connected cracks inside glass, enabling efficient etching with enhanced rates along the modified profile and the fabrication of surface microstructures. We demonstrate diverse groove arrays with profiles of trapezoid, semicircle, and triangle, revealing low roughness around 1.3 μm, a high depth-width ratio of 3:1, and depth up to 300 μm, which underscore broad applications such as fiber packaging.

Keywords: ultrafast laser processing; multi-focus shaping beam; micro-groove; glass

Xu K, Huang PL, Huang LY et al. High-precision multi-focus laser sculpting of microstructured glass. *Opto-Electron Adv* **7**, 240082 (2024).

Introduction

Glass is extensively applied in optical and optoelectronic devices due to its cost-effectiveness, excellent corrosion resistance, and great optical properties. Glass devices with surface structuring like grooves, ranging from tens of micrometers to hundreds of micrometers in scale, find diverse applications. Providing perfect light transmission and high ablation threshold, glass is the predominant material for optical devices, including cylindrical lens arrays[1] and microlens arrays[2] used in three-dimensional displays and beam shaping for consumer electronics, laser processing, and other applications. Additionally, glass exhibits remarkable insulation properties, resulting in minimal electric loss, particularly during high-frequency transformation compared to traditional semiconductors. For instance, glass with V-shaped grooves[3] is widely adopted in optical fiber packaging to meet the increasing demands of mobile devices and the Internet of Things. Besides, glass grooves are employed in microfluidic chips[4], virtual reality display[5] and many other fields, demonstrating a wide range of potential uses.

Fabricating large-area glass grooves with diverse

[1]Department of Mechanical and Energy Engineering, Southern University of Science and Technology, 1088 Xueyuan Avenue, Shenzhen 518055, China; [2]Guangdong Provincial Engineering and Technology Research Center for Ultrafast Laser Micro-Nano Manufacturing Equipment and Technology, Shenzhen Guihua Intelligent Technology Co., Ltd., Shenzhen 518109, China.

†These authors contributed equally to this work.

*Correspondence: SL Xu, E-mail: xusl@sustech.edu.cn

Received: 14 April 2024; Accepted: 22 July 2024; Published online: 9 October 2024

profiles remains a significant challenge owing to glass's hard, brittle physical characteristics, and low heat conductivity resulting in heat and stress concentration. Glass groove fabrication can utilize additive[6,7], formative[8,9], and subtractive manufacturing methods. Three-dimensional printing, as an additive manufacturing approach for glass structuring, offers high shape design flexibility. While it requires a sintering process after solidification due to the addition of silica nanoparticles into photoresist, which may lead to a dimensional shrink causing inaccuracy in scale. As for formative manufacturing, glass molding process is commonly used for glass structuring. The mold fabrication relies on expensive traditional subtractive manufacturing such as highly precision cutting. The molding temperature for fused silica with excellent optical characteristics has to exceed 1500 °C, which is energy consuming and relies on mold material with extremely high melting point.

Subtractive manufacturing is primarily utilized in glass structuring, employing two distinct methods: the contact and non-contact ones. The contact method involves precision cutting with diamond tools, which inevitably leads to tool wear, limiting the lifespan and constraining the groove's shape flexibility. In contrast, non-contact methods use various kinds of "beams" for material removal such as ion beam and laser. Ultrafast laser processing, as a non-contact subtractive method with freeform shape modulating ability, offers significant advantages for glass grooving. The ultrafast laser's extremely high peak power density and short reaction time per pulse boasts a low heat-affected zone, resulting in fewer defects[10,11]. And its small focal spot allows for precise material removal during each ablation, ensuring high precision. Notably, the non-contact ablation process ensures good consistency by avoiding tool wear and tear. Furthermore, ultrafast laser processing, with its versatile electric field modulation capabilities, offers exceptional freedom for achieving varied groove shapes, proving valuable in the efficient fabrication of diverse glass grooves. For instance, the utilization of Bessel beam for creating cylindrical lens arrays[12] has been explored, albeit limited by challenges in achieving large size range, precise shape control, and surface smoothness. In contrast, the implementation of multi-focus light modulation potentially allows for highly efficient surface structure fabrication with high shape controllability, if the multi-focus laser can be arranged along any tailored curves for separating glass. Multi-focus laser irradiation combined with chemical etching has been employed to directly create microlens arrays[13], yet faces limitations in shape control. This multi-focus laser can be realized through advanced techniques such as the superposition of gratings and lenses algorithm (S algorithm)[14], diffraction elements such as Dammann gratings[15], holographic images with Gerchberg-Saxton algorithm[16], and optimal-rotation-angle method[17,18]. Uniform energy distribution and precise scale control guarantee the accurate production of grooves. Unexpected focusing causes energy ununiformity of multi-foci from S algorithm mainly due to Moiré patterns on phase images when points are equidistantly arranged. Several methods are introduced to break the Moiré patterns, including adding additional mild random phase[19] or slight random coordinate displacement of every point along the light propagation direction[20] to improve energy uniformity. As for holographic images, the scale accuracy can be directly improved by experimental iteration. Further aberration correction factors can be introduced into the algorithm to consider the refractive-index-induced deviation[21].

Ablation in laser direct writing for glass crafting results in rough surfaces due to extensive material removal. To achieve three-dimensional structures on glass with reduced roughness, chemical etching is employed to proceed chemical removal of laser-modified materials, ensuring low damage and high precision. Two major types of chemical etching are applied for glass engraving: acid etching (e.g. HF) with low selective etching ratio, and alkaline etching (e.g. KOH) with high selective etching ratio. Laser ablated spot in the glass surface can be the starting seed for HF etching to create a hemispherical crater[22]. Further dot array in line arrangement can help to connect the craters into cylindrical engraved structures[23]. And further 3D multi-focus laser is able to create a crater array in a concave surface[18]. Glass structuring assisted with alkaline etching relies more on laser modified regions due to high selective etching ratio. Laser direct writing offers high degree of freedom in 3D glass structuring[24,25].

We here present a spatial multi-focus laser processing technique to efficiently produce customizable glass grooves with a diverse range of shapes. By employing three-dimensional multi-focus laser beam, we achieve the desired modified sectional profile during a single scanning pass, aided by chemical etching to separate the laser-modulated region and produce the glass grooves. The phase diagrams for multi-focus laser modulation are

calculated by optimized superposition of gratings and lenses. Notably, this algorithm eliminates the need for iterative optimization, ensuring rapid calculations, easy adjustments, and minimal demand for complex numerical processing. This revised algorithm tackles two primary challenges: first, it corrects the position deviation caused by the glass's refractive index and nonparaxial situation through considering more practical optical system during the coordinate calculation. Secondly, it mitigates unexpected energy concentration resulting from circular Moiré patterns on the phase diagram due to uniform focal point arrangement through introducing controlled randomization of designed positions and further energy adjustment point by point. The precise and uniform multi-focus laser distribution follows the well-designed sectional profile, facilitating the subsequent formation of glass groove with high form accuracy through chemical etching. We demonstrate various groove shapes, including large-area trapezoidal grooves, high-aspect-ratio triangle grooves, semicircle grooves and more. Furthermore, we exhibit the practical applications of these glass grooves in optoelectronic devices, showcasing 48-groove fiber-optic packaging with trapezoidal groove arrays.

Experiments

In Fig. 1(a), we utilize an ultrafast laser (Pharos, Light Conversion) operating at a 1030 nm wavelength, featuring a pulse width ranging from 220 fs to 20 ps, and a maximum single pulse energy of 200 μJ. The choice of pulse width is determined by the composition and characteristics of the glass: shorter pulse widths are more suitable for fused silica, while longer pulse widths are better for composite glass to accommodate heavier thermal effect for material bulk ablation. The Gaussian beam is then modulated using a phase diagram on a spatial light modulator (X15213, Hamamatsu), creating a multi-focus laser spot (Fig. 1(b)) with a custom trapezoid-shape distribution. And the beam is subsequently focused using either a 20× objective (with a numerical aperture of 0.45) or a 50× objective (with a numerical aperture of 0.65). Next, the modulated laser is scanned

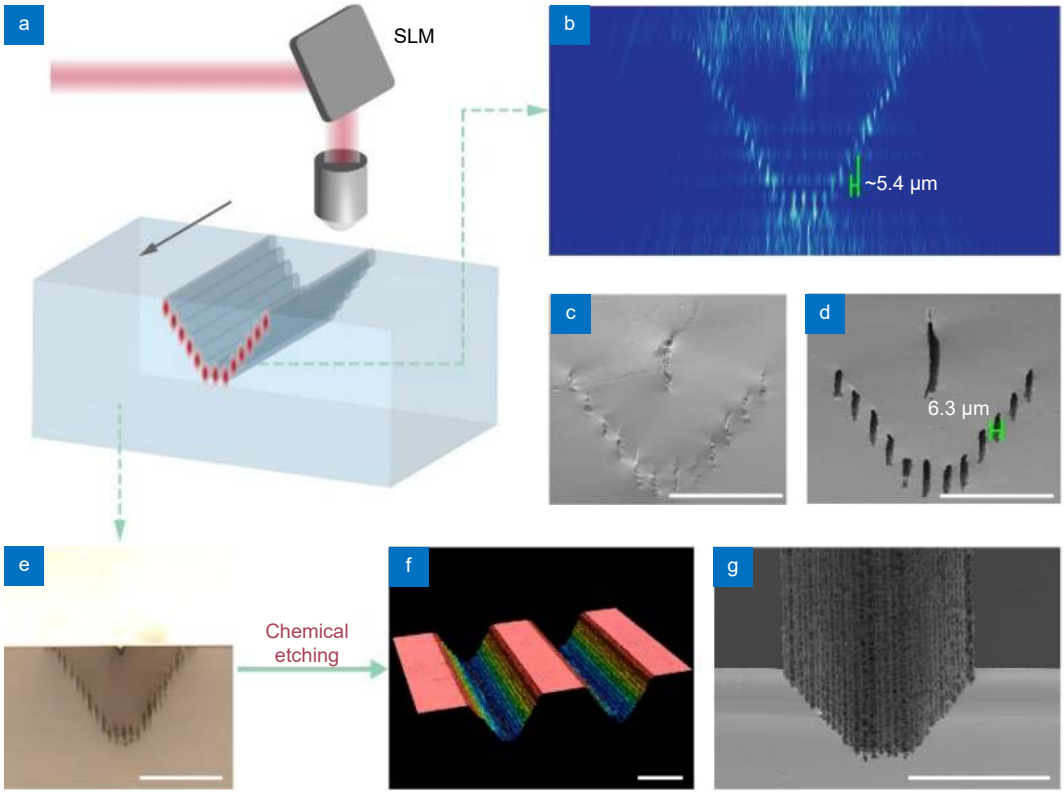

Fig. 1 | Multi-focus laser processing for efficient fabrication of a trapezoid groove. (**a**) Schematic of multi-focus laser processing. (**b**) Simulated light intensity field of multi-focus spot. (**c**) 45° tilted view of multi-focus ablation. (**d**) 45° tilted view of multi-focus ablation after chemical etching. (**e**) Cross-sectional view of the groove on fused silica after laser processing, observed with an optical microscope. (**f**) Three-dimensional view of the groove after chemical etching, captured by laser scanning confocal microscopy. (**g**) 45° tilted view of the groove, imaged with scanning electronic microscope. Scale bars: 100 μm.

across the glass surface at a scanning speed of 10–50 mm/s, with a fixed frequency repetition of 50 kHz. This process induces sequential cracks in the glass (Fig. 1(c,e), S12, S13), resulting in a significantly higher etching rate compared to the original glass. For the final step, we adopt ultrasonic chemical etching with hot KOH (80–90 wt% at 80–90 °C) for 3–6 hours (Fig. 1(d)). During the process, the separate cracks connect under concentrated stress and chemical etching, leading to the separation of the material and the creation of a well-designed trapezoid-shape groove on the glass's surface (Fig. 1(f, g)). The chemical etching finally attains a surface roughness of less than 1.5 μm (Fig. S9, S10). Detailed fabrication parameters are provided in Table S1. To analyze the structure, we use an optical microscope to detect the cross section (Fig. 1(e)), a laser scanning confocal microscope to evaluate the profile and roughness (Fig. 1(f)), and a scanning electron microscope to examine the detailed surface morphology (Fig. 1(g)).

Results and discussion

Optimization of laser focal position in glass

In this work, the phase diagram for arbitrary multi-focus spot is obtained by combining a Fresnel lens and a blaze grating, as detailed in equations[14] in Section 1 of the Supplementary information under the coordinate in Fig. 2(a), and is optimized through taking the glass's refractive index and nonparaxial situation into consideration which is more practical.

Initially, the position error in the z-direction arises from the difference in optical path length between glass and air (Fig. S1). To correct this error, we divide the designed z-coordinate by the refractive index (n), yielding the optimized coordinate z_j'[26]:

$$z_j' = \frac{z_j}{n}\,, \tag{1}$$

where z_j is the target coordinate, and j is the sequence number of the point. Practical fabrication of V-shaped dot arrays (Fig. 2(b)) requires adjustment for the coordinate to achieve the desired angle.

However, as the designed dots move away from the zero point, position errors stemming from the approximations in the deviations of the blaze grating's period and Fresnel lens' focal length become more pronounced (Fig. 2(c)). These errors result from the non-ideal misplacement of the Fresnel lens and objective, and the ignorance of the distance between zero point and designed dot in the classical blaze grating deviations (Fig. S2).

To correct the x and y coordinates, we introduce the ignored distance between zero point and designed dot to the equations[26], derived from Eqs. S8, S9:

$$p_{m,j} = \frac{\lambda}{\sin\left(\arctan\left(\dfrac{m_j}{f_{\mathrm{OB}} + z_j}\right)\right)}\,, \tag{2}$$

where m is x or y denoting sectional displacement, z_j is the z-direction displacement, the λ is the wavelength, f_{OB}

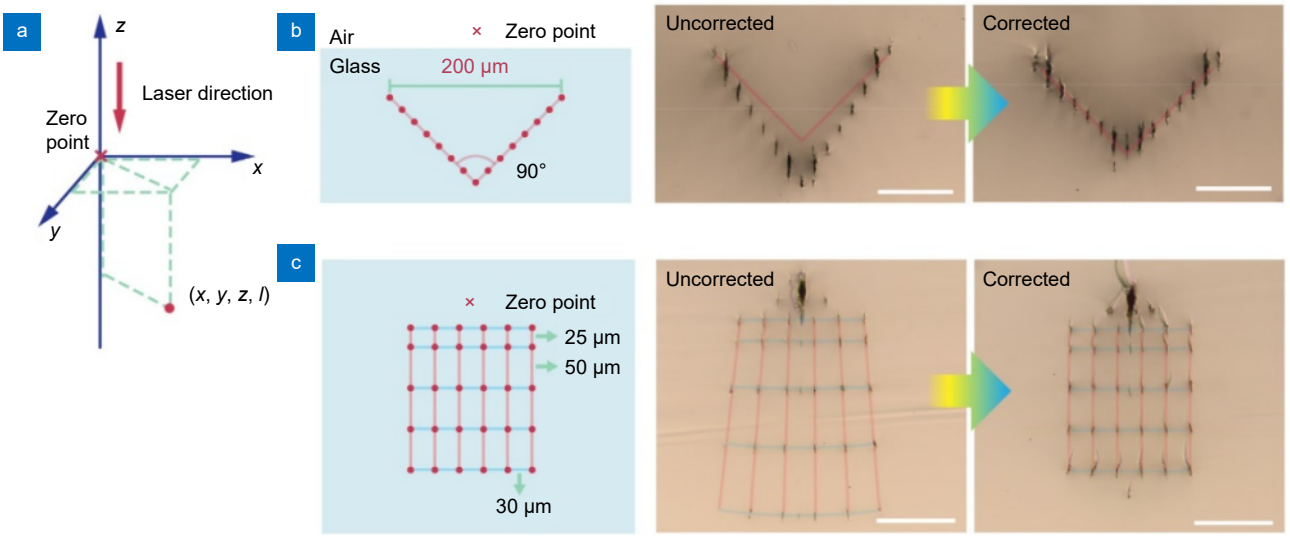

Fig. 2 | Correction of multi-focus modulation. (**a**) Illustration of single-spot coordinate. (**b**) Illustration of V-shaped design (left) and experimental results on fused silica produced by 20× objective without (middle) and with (right) refractive index correction. (**c**) Illustration of designed grid (left) with corresponding experimental results on fused silica produced by 50× objective without (middle) and with (right) complex correction. Scale bars: 100 μm.

is the focal length of objective (10 mm for 20× objective and 4 mm for objective 50×), and p_j is the period of blaze grating.

For further z-direction correction, we consider the practical condition of a fixed distance (d) between the Fresnel lens and objective[26] (Fig. S3), derived from Eq. S10:

$$f_{0,j} = \frac{(f_{\mathrm{OB}} - d)\,(f_{\mathrm{OB}} + z'_j)}{-z'_j}\,, \tag{3}$$

where f_0 is the focal length of Fresnel lens for light modulation, d is the distance between the phase diagram (after 4f system) and the objective, which is constant for the certain optical system.

After applying these corrections, the produced dots closely correspond to the designed dots (Fig. 2(c)). Further correction results produced by the 20× objective are provided in Fig. S4, revealing the same correction process.

Improvement of energy uniformity of multi-focus points

Ensuring both shape accuracy and energy uniformity is crucial for successfully producing the glass groove with continuous sectional lines.

Typically, uniform coordinate arrangements of multi-focus points can lead to detrimental localized energy concentration, resulting in heavy ablation at certain points and weak ablation elsewhere, especially evident when the number of points increases. Figure 3(a, b) demonstrate this energy concentration primarily occurring at the center (position 2) and both sides (position 1),

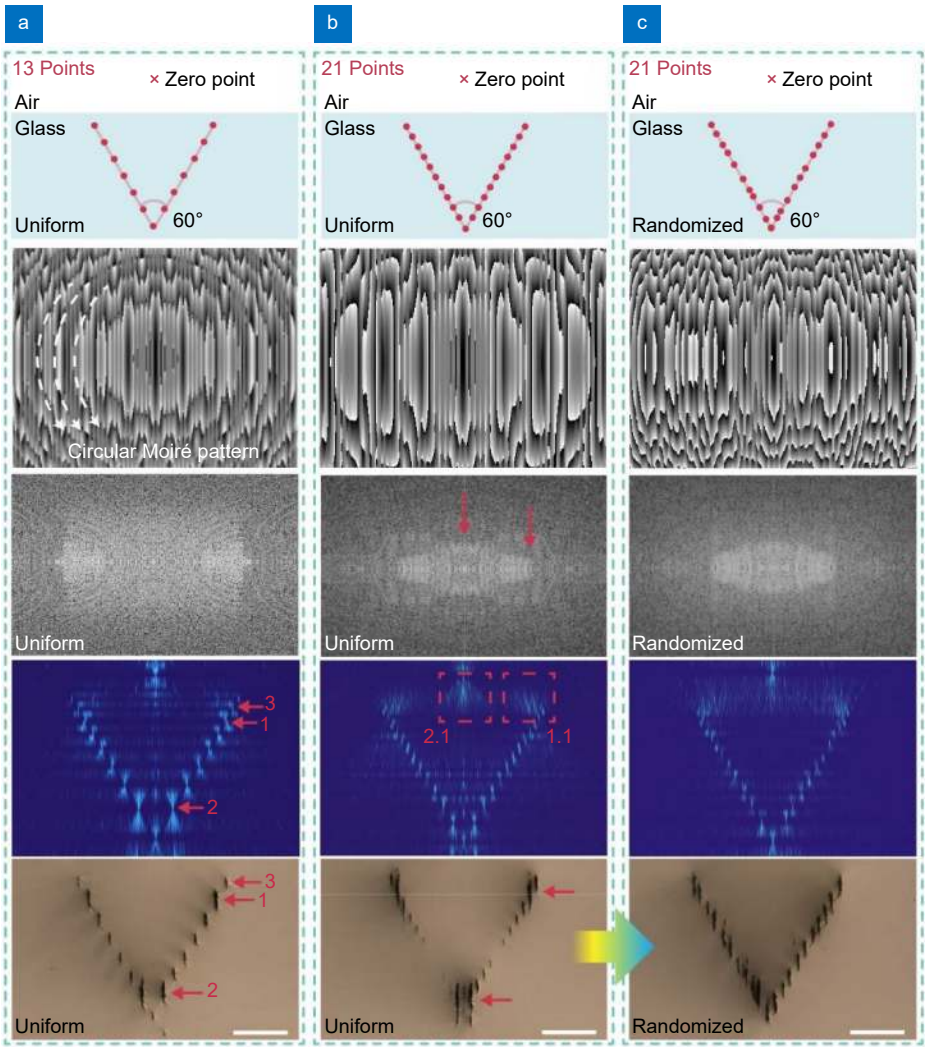

Fig. 3 | Uniformity improving of multi focus by randomization of their coordinates in fused silica. Illustration, phase diagram, fast Fourier transform images of phase diagrams showing circular Moiré patterns, light intensity field simulation, and bulk ablation of V-shape dot array with uniform multi foci of (**a**) 13 points , (**b**) 21 points , and (**c**) 21 points with randomized position. Scale bars: 100 μm.

when the point number increases from 13 to 21. This concentration deprives energy from the middle of the side line, leading to weak ablation, and can cause additional unexpected dots (position 3).

The energy non-uniformity stems from the unintended localized focusing from the phase diagram. A noticeable periodic circular Moiré pattern appears in the phase diagram (Fig. 3(a) and Fig. S5) due to the uniform arrangement of dots, acting as an undesired lens leading to unexpected focus. The concentration is validated by electric field simulations based on diffraction integral theory fast Fourier transform images, and bulk ablation experiments in Fig. 3(a, b)[27], where energy localization occurs during light propagation and becomes more obvious with larger point number (observed in dotted boxes, position 1.1 and 2.1). The circular periodic Moiré pattern in phase diagrams leads to local intensity concentration in the fast Fourier transform, which in turn highlights the unexpected localized light energy concentration, indicating non-uniformity.

To address this issue, we introduce a slight randomization of the coordinate while still preserving the target profiles (Fig. 3(c)), namely introducing a randomization in x or y coordinate and then finding the corresponding counterpart coordinate in the target profile line. The detailed operation process of randomization is stated in Section 1 in Supplementary information. It effectively breaks the circular Moiré pattern caused by regular dot distribution to enhancing the uniformity of fast Fourier transform images and achieving uniformity in light intensity. Larger modulation efficiency with heavier ablation of the multi-focus region under the same fabricating parameters comparing uniform type (Fig. 3(b)) and random type (Fig. 3(c)). After the randomization, a V shape with 21 points is produced, featuring a continuous linear uniform arrangement. The energy localized concentration can be eliminated to some extent through this randomization.

However, when the dot array has extreme locations (Fig. 4(a)) or an excessive number of points, the energy concentration persists, leading to potential cracks caused by concentrated stress during the laser processing and etching. To mitigate this, we propose an energy adjustment method by incorporating an energy-related constant ratio into the amplitude of each transmission function of a single point:

$$T = Ae^{\phi i} = \sum_j \left\{ I_j \times \exp\left[\left(\frac{2\pi r_x}{p_{x,j}} + \frac{2\pi r_y}{p_{y,j}} + \frac{\pi r_0^2}{\lambda f_{0,j}} \right) i \right] \right\} ,$$

where T is the transmission function for the light modulation, A is the amplitude constant (meaningless in this equation), j is the point number, ϕ is the phase forming the phase diagram for light modulation, I_j is normalized energy adjustment coefficient for each point, $p_{x,j}$ and $p_{y,j}$ are the blaze grating period from Eq. (2), r is the distance of each phase pixel from the center of the phase diagram with subscript "x", "y" and "0" indicating the projection in the x or y direction and no projection, and $f_{0,j}$ is the focal length of Fresnel lens from Eq. (3). It is noticed that the trend of energy adjustment coefficient can be determined by the light field intensity simulation, but the accurate value selection should be verified by the corresponding experiments due to complex laser-matter interaction.

After implementing the energy adjustment shown in Fig. 4(a), our proposed method successfully achieves the desired reduction in dot energy at the center and sides of the array. The light intensity field simulations (Fig. 4(b, c)) illustrate the energy reduction at the center and side after adjustment, which match the experimental results (Fig. 4(d, e)).This method of adjustment result in a noticeably more uniform and controllable dot array, finally realizing the suppression of cracks caused by tip energy concentration (Fig. 4(f, g)).

Demonstration of diverse grooves and their applications

Low surface roughness is crucial for great application performance, which can be achieved by improving laser spot intensity uniformity and especially decreasing the point-to-point distance. We employ a multi-focus laser (focused by 20× objective) to manufacture V-shaped grooves (with a width of 200 μm and a base angle of 60°) with uniformity improving operation stated before (Fig. 5(a)). After hot alkaline etching, the modified region separates from the body substrate along the crack, forming V-shaped grooves (Fig. 5(b)) that match well with the designed profile (Fig. 5(c)). As shown in Fig. 5(d), when the quantity of points rises from 33 to 61 denoting reducing of average point-to-point distance from 12.5 to 6.6 μm, the surface roughness decreases at first because that controllable short cracks simultaneously occur

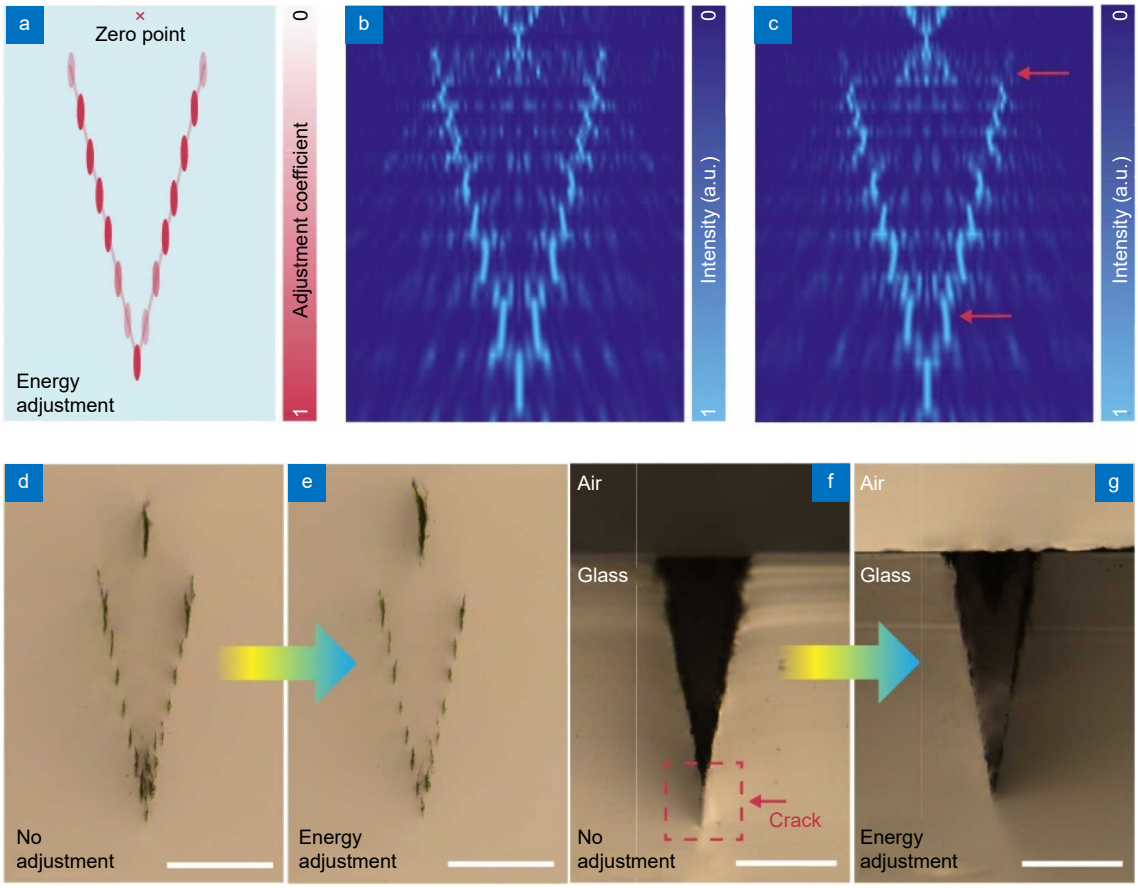

Fig. 4 | Point-by-point energy adjustment of dot array with high aspect ratio. (**a**) Illustration of selection of energy adjustment coefficient. Light intensity field simulation and experimental results on fused silica of 15-point array ablation or 33-point array without (**b**,**d**,**f**) and with energy adjustment (**c**,**e**,**g**). Scale bar: 100 μm.

between points, forming smaller steps and resulting in smoother surface. However, too many points would create a heavy heat effect during ablation causing coarser cracks and worse surface morphology after etching. Besides, increasing point number makes phase images too complex to exceed light modulator's resolution, eliminating the modulating efficiency. Finally, the V-shaped groove processed by a multi-focus beam with 46 foci (namely point-to-point distance of 8.9 μm) presents the minimal surface roughness of 1.6 μm. (Fig. 5(d)).

This method shows extremely high flexibility in shape controllability. We manufacture a variety of V-shaped grooves (Fig. S6, S7) on the glass surface. Notably, we demonstrate the creation of deep V-shaped grooves (Fig. 6(a)) measuring 300 μm in height and 100 μm in width (with depth-width ratio of 3:1), as well as tilted V-shaped grooves with the maximum tilted angle of 135° (Fig. 6(a)). Additionally, we present arc-shaped grooves with a radius of 50 μm (Fig. 6(b)) and cylinder arrays with a period of 100 μm (Fig. 6(c), S8(b)).

The exemplary applications are showcased in the realm of fiber packaging devices. we introduce a fiber array designed for optical fiber packaging (Fig. 6(d), S8(a)). This array features large-area trapezoidal-shape grooves on borosilicate glass (BOROFLOAT 33 from SCOTT, 1.5×5 cm^2, 48 grooves in each period) with a surface roughness of 1.3 μm (Fig. S9) and a shape error of ~4 μm (Fig. S10) to the designed profile.

Conclusions

The fabrication of large-area glass grooves with diverse profiles presents challenges due to glass's inherent hardness, brittleness, and low heat conductivity, leading to heat accumulation and stress concentration. Here, we introduce a novel approach using selective laser modification assisted etching, leveraging a one-step laser modulation with spatial multi-focus technology to directly achieve desired sectional profiles for customizable glass groove fabrication.

The multi-focus laser modulation is realized through

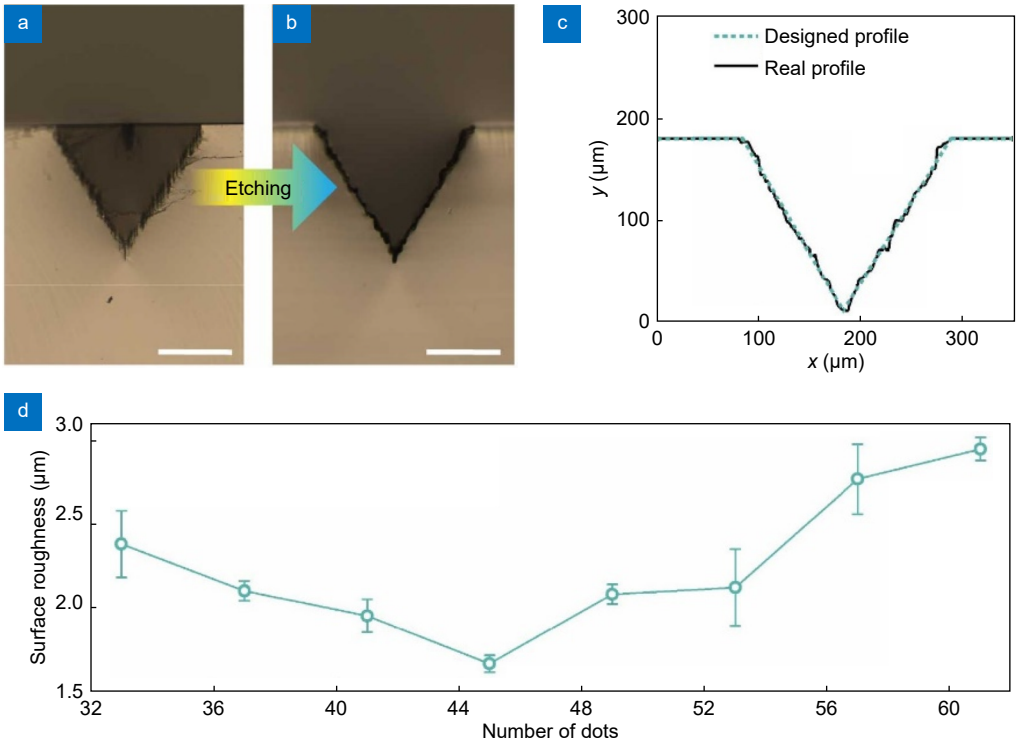

Fig. 5 | The profile and surface roughness of the V-shaped groove. (**a**) A V-shaped modified region processed by a multi-focus beam with 46 foci. (**b**) Etching result of V-shaped groove. (**c**) Designed profile and real profile of V-shaped groove. (**d**) Surface roughness of V-shaped grooves vary with the number of foci. Scale bars: 100 μm.

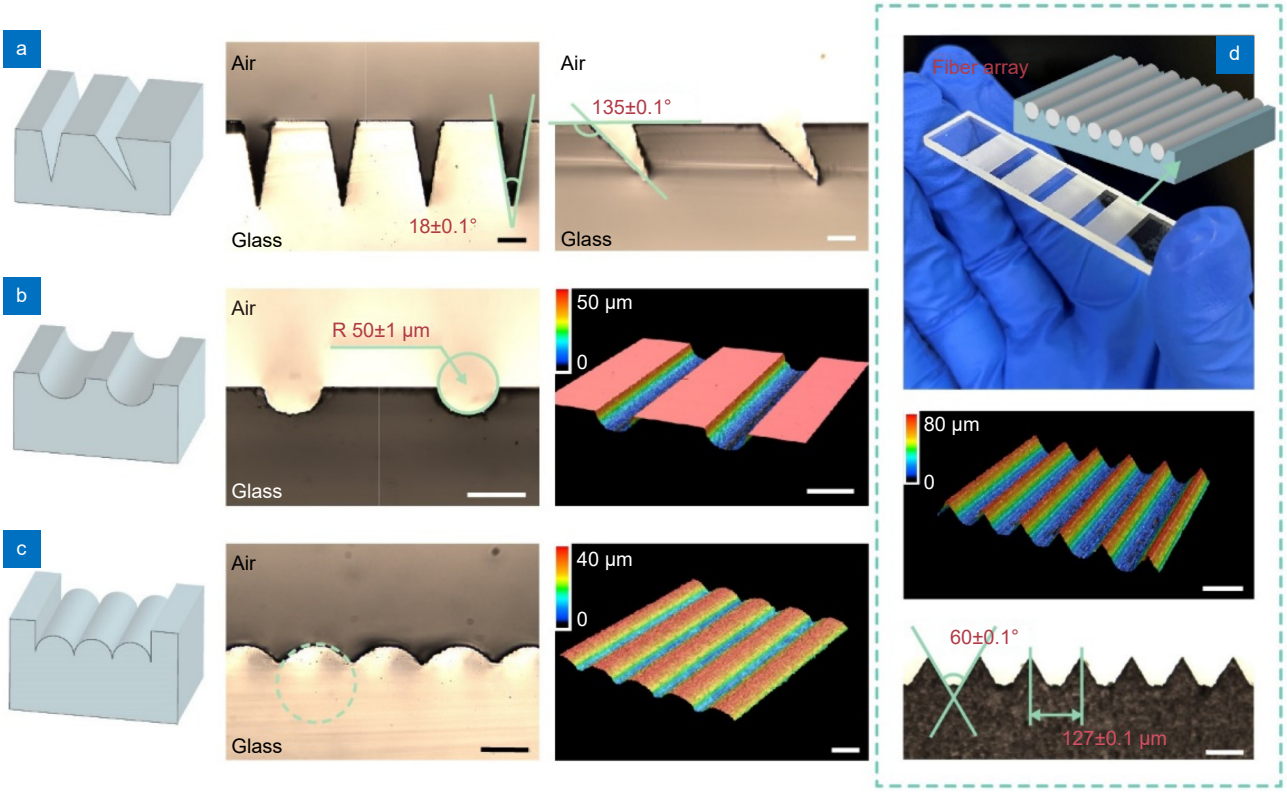

Fig. 6 | Diverse sectional profiles of glass grooves achieved through spatial multi-focus laser processing combined with chemical etching, along with their various applications. (**a**) Symmetric and asymmetric V-shaped grooves on fused silica. (**b**) Arc-shaped grooves on fused silica. (**c**) Cylinder arrays formed by continuous grooves on fused silica. (**d**) Trapezoid grooves on borosilicate glass used for optical fiber packaging. Scale bars: 100 μm.

phase diagrams created by an advanced algorithm based the superposition of Fresnel lens and blaze gratings with optimizing formulas and strategies. This sophisticated algorithm accurately corrects position deviations resulting from the glass's refractive index and nonparaxial situation, employing optimized coordinate calculations. And it effectively deals with the un-uniformity of each point's energy stemming from circular Moiré patterns on the phase diagram through strategic randomization of designed positions and precise energy adjustments point by point.

To selectively etch the modulated region and create the glass grooves, we employ alkaline chemical etching. A precisely designed and uniform multi-focus laser is achieved, with points' distribution following well-designed sectional profile, facilitating the subsequent glass groove formation through chemical etching.

We demonstrate the fabrication of large-area trapezoidal grooves, high-aspect-ratio triangle grooves, semicircle grooves and more, revealing extremely high flexibility in shape control of glass grooves of this method. Additionally, we showcase a 48-groove fiber-optic packaging device utilizing trapezoidal groove arrays. The trapezoidal groove array has surface roughness of 1.3 μm and shape error of 4 μm to the designed one, potentially replacing those of mechanically fabricated ones.

References

1. Luo Z, Yin K, Dong XR et al. Fabrication of parabolic cylindrical microlens array by shaped femtosecond laser. *Opt Mater* **78**, 465–470 (2018).
2. Yuan W, Li LH, Lee WB et al. Fabrication of microlens array and its application: a review. *Chin J Mech Eng* **31**, 16 (2018).
3. Ha TW, Heo GS, Choi BH et al. Wafer-level fabrication of a high-silica v-groove for fiber-optic packaging using deep dry-etching with a dual-frequency high-density plasma. *J Korean Phys Soc* **67**, 1179–1186 (2015).
4. Gottmann J, Hermans M, Repiev N et al. Selective laser-induced etching of 3D precision quartz glass components for microfluidic applications—up-scaling of complexity and speed. *Micromachines* **8**, 110 (2017).
5. Xiong JH, Hsiang EL, He ZQ et al. Augmented reality and virtual reality displays: emerging technologies and future perspectives. *Light Sci Appl* **10**, 216 (2021).
6. Wen XW, Zhang BY, Wang WP et al. 3D-printed silica with nanoscale resolution. *Nat Mater* **20**, 1506–1511 (2021).
7. Toombs JT, Luitz M, Cook CC et al. Volumetric additive manufacturing of silica glass with microscale computed axial lithography. *Science* **376**, 308–312 (2022).
8. Zhou TF, Liu XH, Liang ZQ et al. Recent advancements in optical microstructure fabrication through glass molding process. *Front Mech Eng* **12**, 46–65 (2017).
9. Zhou TF, He YP, Wang TX et al. A review of the techniques for the mold manufacturing of micro/nanostructures for precision glass molding. *Int J Extrem Manuf* **3**, 042002 (2021).
10. Zhang B, Wang Z, Tan DZ et al. Ultrafast laser-induced self-organized nanostructuring in transparent dielectrics: fundamentals and applications. *PhotoniX* **4**, 24 (2023).
11. Wang Z, Zhang B, Wang ZQ et al. 3D imprinting of voxel-level structural colors in lithium niobate crystal. *Adv Mater* **35**, 2303256 (2023).
12. Luo Z, Duan J, Guo CL. Femtosecond laser one-step direct-writing cylindrical microlens array on fused silica. *Opt Lett* **42**, 2358–2361 (2017).
13. Pan A, Chen T, Li CX et al. Parallel fabrication of silicon concave microlens array by femtosecond laser irradiation and mixed acid etching. *Chin Opt Lett* **14**, 052201 (2016).
14. Liesener J, Reicherter M, Haist T et al. Multi-functional optical tweezers using computer-generated holograms. *Opt Commun* **185**, 77–82 (2000).
15. Zhou C, Liu L. Numerical study of dammann array illuminators. *Appl Opt* **34**, 5961–5969 (1995).
16. Yang GZ, Dong BZ, Gu BY et al. Gerchberg–Saxton and Yang–Gu algorithms for phase retrieval in a nonunitary transform system: a comparison. *Appl Opt* **33**, 209–218 (1994).
17. Takahashi H, Hasegawa S, Hayasaki Y. Holographic femtosecond laser processing using optimal-rotation-angle method with compensation of spatial frequency response of liquid crystal spatial light modulator. *Appl Opt* **46**, 5917–5923 (2007).
18. Wang L, Gong W, Cao XW et al. Holographic laser fabrication of 3D artificial compound μ-eyes. *Light Adv Manuf* **4**, 26 (2023).
19. Lesem LB, Hirsch PM, Jordan JA. The kinoform: a new wavefront reconstruction device. *IBM J Res Dev* **13**, 150–155 (1969).
20. Curtis JE, Schmitz CHJ, Spatz JP. Symmetry dependence of holograms for optical trapping. *Opt Lett* **30**, 2086–2088 (2005).
21. Jesacher A, Booth MJ. Parallel direct laser writing in three dimensions with spatially dependent aberration correction. *Opt Express* **18**, 21090–21099 (2010).
22. Chen F, Liu HW, Yang Q et al. Maskless fabrication of concave microlens arrays on silica glasses by a femtosecond-laser-enhanced local wet etching method. *Opt Express* **18**, 20334–20343 (2010).
23. Wu PC, Cao XW, Chen ZH et al. Fabrication of cylindrical microlens by femtosecond laser-assisted hydrofluoric acid wet etching of fused silica. *Adv Photonics Res* **4**, 2200227 (2023).
24. Kim S, Kim J, Joung YH et al. Optimization of selective laser-induced etching (SLE) for fabrication of 3D glass microfluidic device with multi-layer micro channels. *Micro Nano Syst Lett* **7**, 15 (2019).
25. Bischof D, Kahl M, Michler M. Laser-assisted etching of borosilicate glass in potassium hydroxide. *Opt Mater Express* **11**, 1185–1195 (2021).
26. Pedrotti FL, Pedrotti LM, Pedrotti LS. *Introduction to Optics* 3rd ed (Cambridge University Press, Cambridge, 2017).
27. Huang LY, Xu K, Yuan DD et al. Sub-wavelength patterned pulse laser lithography for efficient fabrication of large-area metasurfaces. *Nat Commun* **13**, 5823 (2022).

Acknowledgements

This work was financially supported by the National Natural Science Foundation of China (Grant No. 52375438), the Shenzhen Science and Technology Programs (Grant No. JCYJ20220818100408019, JSGG20220831101401003), and Jiangyin-SUSTech Innovation Fund.

The authors wish to thank the Materials Characterization and Preparation Center of Southern University of Science and Technology for the SEM characterization.

Author contributions

K. Xu processed the experiments, carried out the optical simulations, and wrote the paper. P. L. Huang provided the optimization for phase diagrams, and processed the sample fabrication. L. Y. Huang, L. Yao and J. T. Chen processed the experiments. L. Y. Huang revised the manuscript. S. L. Xu leaded the projects and revised the paper. All authors contributed to scientific discussion.

Competing interests

The authors declare no competing financial interests.

Supplementary information

Supplementary information for this paper is available at https://doi.org/10.29026/oea.2024.240082

Scan for Article PDF